

Spin dynamics and domain formation of a spinor Bose-Einstein condensate in an optical cavity

Lu Zhou,¹ Han Pu,² Hong Y. Ling,³ Keye Zhang,¹ and Weiping Zhang¹

¹State Key Laboratory of Precision Spectroscopy, Department of Physics, East China Normal University, Shanghai 200062, China

²Department of Physics and Astronomy, and Rice Quantum Institute, Rice University, Houston, Texas 77251-1892, USA

³Department of Physics and Astronomy, Rowan University, Glassboro, New Jersey 08028-1700, USA

(Received 11 May 2010; published 30 June 2010)

We consider a ferromagnetic spin-1 Bose-Einstein condensate (BEC) dispersively coupled to a unidirectional ring cavity. We show that the ability of the cavity to modify, in a highly nonlinear fashion, matter-wave phase shifts adds an additional dimension to the study of spinor condensates. In addition to demonstrating strong matter-wave bistability as in our earlier publication [L. Zhou *et al.*, *Phys. Rev. Lett.* **103**, 160403 (2009)], we show that the interplay between atomic and cavity fields can greatly enrich both the physics of critical slowing down in spin-mixing dynamics and the physics of spin-domain formation in spinor condensates.

DOI: [10.1103/PhysRevA.81.063641](https://doi.org/10.1103/PhysRevA.81.063641)

PACS number(s): 03.75.Mn, 03.75.Kk, 42.50.Pq, 42.65.-k

I. INTRODUCTION

Experimental realization of spinor Bose-Einstein condensates (BECs) has opened up a new research direction of cold atom physics [1], in which superfluidity and magnetism are simultaneously realized. Compared to scalar condensates, spinor condensates possess unique features: (i) The spin-dependent collision interactions allow for the population exchange among hyperfine spin states; (ii) The spinor condensate is described by an order parameter with vector character and therefore may exhibit spontaneous magnetic ordering. These give rise to spin-dependent phenomena such as coherent spin mixing, spin textures and vortices, spin waves, and spin domains. These phenomena have been demonstrated by many pioneering experimental works [1–8] and extensively studied in theory [9–22].

In the study of spinor BEC, it has been found that magnetic field plays an important role, particularly via the quadratic Zeeman effect. Coherent control of the spin-dependent behavior has been achieved by tuning magnetic field. These include the control of the oscillation period and amplitude of coherent spin mixing [3–5, 12–15], formation of spin-domain structure [1–3, 18–22], and quantum phase transitions between different magnetically ordered states [2, 8, 11].

In another frontier of cold atom research, recent experimental progress has realized strong coupling of BEC to electromagnetic modes of optical cavity [23, 24]. This heralds a new regime of cavity quantum electrodynamics, where a cavity field at the level of a single photon can significantly affect the collective motion of the atomic samples, hence opening up new possibilities in manipulating ultracold atomic gases with cavity-mediated nonlinear interaction. Previous works focused on the interplay between the cavity field and the atomic external degrees of freedom—the center-of-mass motion of scalar condensates [25–33]. The ground-state and collective excitations [28, 29], cavity-induced Mott-insulator–superfluid phase transition [32], and cavity optomechanics [33] were theoretically investigated in detail. Such a system was also shown to have the potential applications in probing atomic quantum statistics in optical lattices and atomic quantum state preparation [34]. Experimentally, optical bistability at few-photon level has been observed, which is made possible by the strong atom-photon coupling [25, 27].

In our recent work [35], a system of a spin-1 BEC trapped inside a unidirectional ring cavity was studied, where the cavity couples to the atomic internal spin degrees of freedom. We examined the equilibrium properties of this system under the single-mode approximation (SMA)—where all three atomic spin states are described by the same spatial wave function—and showed that the interplay between the atomic spin mixing and the cavity light field can lead to strong matter wave and optical bistability simultaneously. Our current work is an extension of Ref. [35]. Here we will conduct a more thorough investigation by including the study of the nonequilibrium properties and the collective excitations of the system. We will also examine the validity of the SMA for atomic wave functions and show that, when the SMA becomes invalid, spatial domain structure will form in the spinor condensate. This spin-domain formation is initiated by the modulational instability induced by the cavity light field. It adds an alternative route toward spin-domain formation besides the use of magnetic field. This study will help us gain insight into such properties as the spinor dynamics, dynamical stability, spin-domain formation, etc.

The rest of the paper is organized as follows. Sec. II introduces the theoretical model. Sec. III is devoted to a discussion of spinor dynamics under the SMA, where both equilibrium and nonequilibrium properties are studied. The validity of the SMA is examined in Sec. IV by investigating the modulational stability of a homogeneous system. We then present results showing the formation of spin-domain structure in the ground state in a regime where the SMA becomes invalid. Finally we conclude in Sec. V.

II. MODEL

Figure 1 is a schematic of our model in which a spinor BEC with hyperfine spin $F_g = 1$ confined in an optical dipole trap by a spin-independent trapping potential $V_T(\mathbf{r})$ is placed inside a unidirectional ring cavity. The cavity is driven by a coherent laser field with amplitude ε_p and frequency ω_p , far detuned away from the $F_g = 1 \leftrightarrow F_e = 1$ atomic transition with transition frequency ω_a such that the atom-photon interaction is essentially of dispersive nature. Further, the cavity is assumed to support a single π -polarized electromagnetic mode characterized by a frequency ω_c and

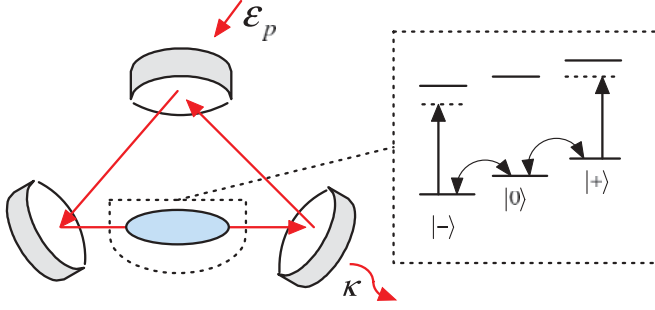


FIG. 1. (Color online) Schematic diagram showing the system under consideration. An $F = 1$ spinor condensate is trapped inside the cavity using an optical dipole trap. The population of different spin components can exchange via spin mixing. The cavity is coherently driven by an external laser with amplitude ε_p and decays with a rate κ . The cavity field is π polarized and is dispersively coupled to the atomic system.

a decay rate κ . The selection rule then allows states $|F_g = 1, m_g = \pm 1\rangle$ to be coupled to the corresponding states in the excited manifold with the same magnetic quantum numbers $|F_e = 1, m_e = \pm 1\rangle$, while it forbids state $|F_g = 1, m_g = 0\rangle$ to make dipole transitions to any excited states as shown in Fig. 1. However, population in state $|F_g = 1, m_g = 0\rangle$ can be distributed to other sublevels via the two-body s -wave spin exchange collisions. The total s -wave interaction is described by two numbers, $c_0 = 4\pi\hbar^2(2a_2 + a_0)/3m_a$ and $c_2 = 4\pi\hbar^2(a_2 - a_0)/3m_a$, where m_a is the atom mass, and a_f is the s -wave scattering lengths in the hyperfine channel with a total spin $f = 0$ or 2 . Since the antiferromagnetic case of ^{23}Na has been considered in our previous work [35], here we will focus on the ferromagnetic case of ^{87}Rb spin-1 BEC where $c_2 < 0$. As we shall see, qualitatively similar results are obtained in both cases, indicating that the bistability discussed here is a rather general phenomenon insensitive to the specific atomic system.

In this work, we take the standard mean-field approach, describing the cavity field with a complex amplitude $\alpha(t)$ which amounts to assuming the cavity field to be represented by a coherent state, and the spinor condensate with the order parameters $\psi_-(\mathbf{r}, t)$, $\psi_0(\mathbf{r}, t)$, and $\psi_+(\mathbf{r}, t)$, which represent the wave functions in magnetic sublevels $m_g = -1, 0$, and $+1$, respectively. This treatment is justified when the condensate atom number $N_\alpha = \int n_\alpha(\mathbf{r}) d\mathbf{r}$ (where $n_\alpha = |\psi_\alpha|^2$ is the atom number density) in magnetic sublevel α are sufficiently large. The equations of motion then read

$$i\hbar\dot{\psi}_\pm = [\mathcal{L} + U_0|\alpha|^2 + c_2(n_\pm + n_0 - n_\mp)]\psi_\pm + c_2\psi_0^2\psi_\mp^*, \quad (1a)$$

$$i\hbar\dot{\psi}_0 = [\mathcal{L} + c_2(n_+ + n_-)]\psi_0 + 2c_2\psi_+\psi_-\psi_0^*, \quad (1b)$$

$$\dot{\alpha} = [i\delta_c - iU_0(N_+ + N_-) - \kappa]\alpha + \varepsilon_p, \quad (1c)$$

where $\mathcal{L} = \hat{p}^2/2m_a + V_T(\mathbf{r}) + c_0n$ is the spin-independent part of the Hamiltonian, $n = n_+ + n_0 + n_-$ is the total atomic density, $\delta_c = \omega_p - \omega_c$ is the cavity detuning relative to the external laser field, and $U_0 = g^2/(\omega_p - \omega_a)$ is the effective atom-photon coupling, with g being atom-cavity mode coupling constant. Further, since the cavity decay rate κ is typically much larger than the spin oscillation frequency,

in what follows, we adiabatically eliminate α from Eq. (1c), replacing α in Eq. (1a) with

$$\alpha(t) = \frac{\varepsilon_p}{\kappa - i[\delta_c - U_0(N_+ + N_-)]}. \quad (2)$$

One may immediately observe from Eq. (1) that the dispersive interaction between cavity photons and the condensate atoms introduces an ac Stark shift, $U_0|\alpha|^2$, to $m_g = \pm 1$ states relative to the $m_g = 0$ state. This can be regarded as an effective quadratic Zeeman energy shift. However, unlike the Zeeman shift due to an external magnetic field or to a strong off-resonant laser field [17], a key feature of the cavity-induced effective shift is that it is sensitive to the spin population distribution of the condensate, as manifested by Eq. (2). As such, it generates a new effective spin-dependent interaction which in turn induces a new set of nonlinear phenomena in spinor condensate. In what follows, we will describe in detail such new phenomena.

III. SPIN DYNAMICS UNDER SMA

In this section, we consider the spin dynamics under the assumption of the SMA. This describes, for example, a condensate whose size is smaller than the spin healing length ξ_s defined as $\xi_s = \hbar/\sqrt{2m_a|c_2|n}$ which represents a length scale over which a local perturbation in spin density gets forgotten. Under the SMA, each spin component shares the same spatial wave function $\phi(\mathbf{r})$ according to

$$\psi_\alpha(\mathbf{r}, t) = \sqrt{N}\phi(\mathbf{r})\sqrt{\rho_\alpha(t)}\exp\{-i[\mu t + \theta_\alpha(t)]\}, \quad \alpha = \pm, 0, \quad (3)$$

where $\theta_\alpha(t)$ is the phase, $\rho_\alpha(t)$ is the population normalized with respect to the total atom number $N = \sum_\alpha N_\alpha$, and $\phi(\mathbf{r})$ is the solution to the time-independent Gross-Pitaevskii equation, $\mathcal{L}\phi = \mu\phi$, where μ is the chemical potential and $\phi(\mathbf{r})$ satisfy the normalization condition $\int d\mathbf{r}|\phi(\mathbf{r})|^2 = 1$.

By inserting Eq. (3) into Eqs. (1a) and (1b), we arrive at a set of equations:

$$\frac{d\rho_0}{d\tau} = 2\lambda_a\rho_0\sqrt{(1-\rho_0)^2 - m^2}\sin\theta, \quad (4a)$$

$$\frac{d\theta}{d\tau} = -2\frac{\bar{U}_0|\alpha|^2}{N} + 2\lambda_a \times \left[1 - 2\rho_0 + \frac{(1-\rho_0)(1-2\rho_0) - m^2}{\sqrt{(1-\rho_0)^2 - m^2}}\cos\theta \right], \quad (4b)$$

which describe the spin-mixing dynamics, where $\theta = 2\theta_0 - \theta_+ - \theta_-$ is the relative phase, $m = \rho_+ - \rho_-$ the magnetization, and $\tau = \kappa t$ the dimensionless time. In Eq. (4), we have also introduced other dimensionless quantities given by

$$\lambda_a = \frac{Nc_2 \int d\mathbf{r}|\phi(\mathbf{r})|^4}{\kappa}, \quad \bar{U}_0 = \frac{NU_0}{\kappa}, \quad \eta = \frac{\varepsilon_p}{\kappa}, \quad \bar{\delta}_c = \frac{\delta_c}{\kappa}.$$

To facilitate our study below, we follow Refs. [13,36] and use $d\rho_0/d\tau = -2\partial H/\partial\theta$ and $d\theta/d\tau = 2\partial H/\partial\rho_0$ to construct, in terms of two conjugate variables ρ_0 and θ , the following mean-field Hamiltonian H :

$$H = \lambda_a\rho_0 [1 - \rho_0 + \sqrt{(1-\rho_0)^2 - m^2}\cos\theta] + U(\rho_0), \quad (5)$$

where

$$U(\rho_0) = \frac{\eta^2}{N} \arctan [\bar{U}_0(1 - \rho_0) - \bar{\delta}_c]$$

represents the cavity-mediated atom-atom interaction.

A. Equilibrium property: bistability

In this subsection, we will use Eq. (4) to study the equilibrium property of a condensate in the parameter regime that supports bistability. As can be seen from Eq. (4a), at steady state, there are two branches of stationary solutions: one with $\theta = 0$ (the in-phase state) and the other with $\theta = \pi$ (the out-of-phase state). The in-phase state always has a lower energy for $c_2 < 0$ and we will therefore only focus on the in-phase state in this work. In addition, we will restrict ourselves to the case with zero magnetization $m = 0$ (i.e., we only consider the case where there are equal numbers of $m_g = 1$ and $m_g = -1$ atoms).

Under these conditions, the intracavity photon number can be found, by combing the stationary solution of Eq. (4b) with Eq. (2), to obey the following transcendental equation:

$$|\alpha|^2 = \frac{\eta^2}{1 + (\Delta + \chi|\alpha|^2)^2},$$

where $\Delta = \bar{U}_0/2 - \bar{\delta}_c$ and $\chi = \bar{U}_0^2/4N\lambda_a$. It is well known that when $\eta^2|\chi| > 8\sqrt{3}/9$, the system will display bistable behavior [37].

Figure 2(a) shows how the intracavity photon number changes with detuning $\bar{\delta}_c$, based on a set of realistic parameters: $\lambda_a = -6.8 \times 10^{-5}$ [38], $\bar{U}_0 = -5$, $\eta^2 = 5$, and $N = 2 \times 10^5$.

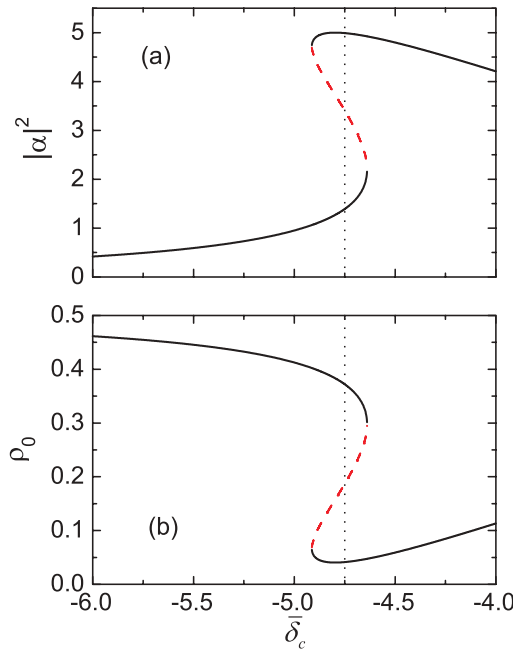


FIG. 2. (Color online) (a) Mean intracavity photon number $|\alpha|^2$ and (b) the normalized spin-0 population ρ_0 versus cavity-pump detuning $\bar{\delta}_c$ for a steady-state solution with $\theta = 0$. The ones represented by the red dashed lines correspond to dynamically unstable solutions. The vertical dotted lines indicate the position of the first-order transition which occurs at $\bar{\delta}_c = -4.75$.

With this set of parameters, $\eta^2|\chi|$ is found to be around 2.3, which is above the threshold value $8\sqrt{3}/9 \approx 1.54$ for bistability to take place. Indeed, for $-4.9 < \bar{\delta}_c < -4.6$, the system supports three stationary solutions. The dynamical properties of these solutions can be studied with the standard linear stability analysis. Substituting $\rho_0 = \rho_0^s + \delta\rho_0$ and $\theta = \theta^s + \delta\theta$ (ρ_0^s is the stationary solution with $\theta^s = 0$) into Eq. (4) and keeping terms up to the first order in fluctuations ($\delta\rho_0, \delta\theta$), we have

$$\begin{aligned} \frac{d}{d\tau} \delta\rho_0 &= 2\lambda_a \rho_0^s (1 - \rho_0^s) \delta\theta, \\ \frac{d}{d\tau} \delta\theta &= -2 \left(4\lambda_a + \frac{\bar{U}_0}{N} \frac{\partial |\alpha|^2}{\partial \rho_0} \Big|_{\rho_0=\rho_0^s} \right) \delta\rho_0, \end{aligned}$$

from which we find the small oscillation frequency ω as determined by the following equation:

$$\omega^2 = 4\lambda_a \rho_0^s (1 - \rho_0^s) \left(4\lambda_a + \frac{\bar{U}_0}{N} \frac{\partial |\alpha|^2}{\partial \rho_0} \Big|_{\rho_0=\rho_0^s} \right).$$

In order to assure the dynamical stability of the system, ω^2 should be positive. We find that in the region with three solutions, two of them are dynamically stable while the third one is dynamically unstable. This unstable state is shown by the red dashed line in Fig. 2; it links the two stable ones, representing a typical example of bistability.

In the region where the intracavity photon number is low, the interaction is dominated by the intrinsic s -wave scattering, which favors the ferromagnetic state in which $\rho_0 = 0.5$ for $m = 0$. In the region where the photon number is high, the cavity-induced effective Zeeman effect takes a more prominent role which, for the choice of $U_0 < 0$, favors a condensate in the $m_g = \pm 1$ magnetic sublevels in which ρ_0 becomes small. If α is fixed to a value independent of the atomic dynamics as in the case when it represents a strong off-resonant laser field [17], the system will experience a smooth crossover from the ferromagnetic-interaction-dominated phase to the Zeeman-effect-dominated phase as the strength of U_0 is tuned. In our case, however, there is a first-order transition located within the bistable region as indicated in Fig. 2. This phase transition exists as a result of the cavity-mediated nonlinear atom-atom interaction.

B. Non-equilibrium property: critical slowing down

In this subsection, we study the spin-mixing dynamics of the system initially prepared in a state away from equilibrium. To begin with, we make use of Eq. (5) and rewrite Eq. (4a) for $m = 0$ as

$$\left(\frac{d\rho_0}{d\tau} \right)^2 = 8\lambda_a \rho_0 (1 - \rho_0) [H - U(\rho_0)] - 4[H - U(\rho_0)]^2, \quad (6)$$

where H is the energy of the system which is a constant determined by the initial condition. In the cavity-free model when U represents a constant quadratic Zeeman shift independent of ρ_0 , Eq. (6) is known to support analytical solutions in the form of elliptic functions [13]. In our case, we have to resort to numerics to solve the above equation. As the system is conservative, the spin dynamics is expected to feature

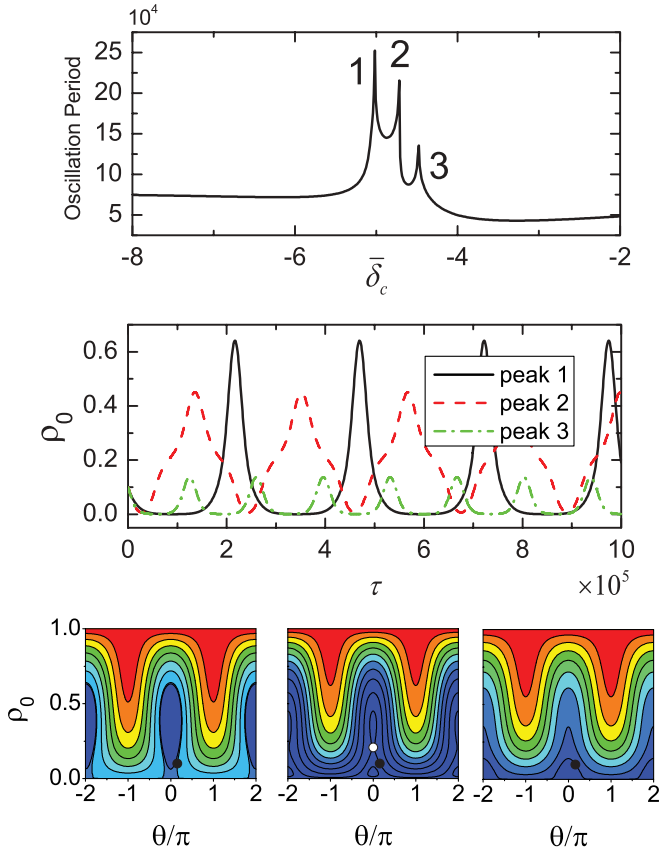


FIG. 3. (Color online) (Top panel) Period of spin oscillations as a function of cavity-pump detuning $\bar{\delta}_c$. (Middle panel) The anharmonic time evolution of ρ_0 for the three peaks marked in the top panel. (Bottom panel) From left to right, the phase-space contour plot of H corresponding, respectively, to the peak 1, 2, and 3 marked in the top panel. The black dots refer to the initial state of the system, while the white dots refer to dynamically unstable fixed points.

periodic population exchanges among different spin states, as in the cavity-free model with a homogeneous magnetic field [13,14].

Figure 3 shows how the oscillation period changes with cavity detuning $\bar{\delta}_c$, where the period is obtained by solving Eq. (6) numerically starting from the initial condition ($\rho_0 = 0.1, \theta = 0.16\pi$) under the same set of parameters that resulted in the equilibrium state in Fig. 2 with $\theta = 0$. Here, cavity detuning $\bar{\delta}_c$ serves as a control knob with which the departure between the initial nonequilibrium state ($\rho_0 = 0.1, \theta = 0.16\pi$) and the closest equilibrium state (an in-phase state with $\theta = 0$) can be conveniently tuned. It plays a similar role as the magnetic field in the study of spin dynamics in the presence of a homogeneous magnetic field. In the ferromagnetic case, it has been theoretically predicted [13] that there is a *single* critical magnetic field around which oscillation period diverges. In contrast, the period as a function of $\bar{\delta}_c$ in Fig. 3 exhibits three peaks around which the period (or the oscillation) experiences a dramatic enhancement (or slowing down).¹

¹This critical slowing down should not be confused with those discussed in [39], in which it refers to an extremely slow return of the system to equilibrium in the vicinity of the bistable transition points.

The spin population ρ_0 as functions of time at three peaks are illustrated in Fig. 3.

To gain physical insights into these dynamics, we plot in the bottom of Fig. 3 the corresponding equal- H contour diagrams in the phase space defined by the conjugate pair (θ, ρ_0) . In a dissipationless system like ours, no matter how complicated the system dynamics may look in the time domain, it evolves along one such contour determined by the initial state (marked as a black dot in Fig. 3). The critical slowing down takes place when the energy approaches a critical value H_c below which the contour changes its topology from an open to a closed line. In the pendulum analogy, it corresponds to the pendulum approaching the vertical upright position. The existence of a bistable region in our example makes the phenomenon of critical slowing down far richer. As can be seen, both the first and third peaks are located outside the bistable region, where only one attractor representing the stable state at $\theta = 0$ exists, while the second one is inside the bistable region, where an unstable saddle point marked by a white dot coexists with two attractors at $\theta = 0$. Our results show that the oscillation period strongly depends on the cavity light field, and the pump field can thus serve as a control knob for the spin-mixing dynamics.

IV. BEYOND SMA

So far we have focused our discussion within the SMA. In this section, we will investigate the validity of the SMA and study the properties of the system when the SMA becomes invalid.

A. Modulational instability of a homogeneous condensate

In order to gain some physical insights into the validity of the SMA, we first consider the case without the trapping potential and assume that the condensate inside the cavity is homogeneous. In this case we have $\psi_\alpha = \sqrt{n_\alpha} \exp(-i\mu_\alpha t - i\theta_\alpha)$, where the atomic density n_α now becomes position independent, and the stationary solution $(n_\alpha^s, \theta_\alpha^s)$ is still determined by Eq. (4) at steady state except that λ_a should be redefined as $\lambda_a \equiv c_2 n / \kappa$.

In order to check whether these homogeneous states are stable against spatial modulation, we examine the Bogoliubov collective excitation spectrum by introducing small fluctuations around the steady-state solution. Inserting $\psi_\alpha = (\sqrt{n_\alpha^s} + \delta\psi_\alpha) \exp(-i\mu_\alpha^s t - i\theta_\alpha^s)$ into Eq. (1), where $\delta\psi_\alpha$ can be expanded in momentum space as $\delta\psi_\alpha(\mathbf{r}, t) = \sum_{\mathbf{k}} [u_\alpha(t) \exp(i\mathbf{k} \cdot \mathbf{r}) + v_\alpha^*(t) \exp(-i\mathbf{k} \cdot \mathbf{r})]$, we obtain a matrix equation $id\mathbf{x}/dt = \mathcal{M}\mathbf{x}$ for vector $\mathbf{x} = (u_+, u_0, u_-, v_+^*, v_0^*, v_-^*)^T$ where \mathcal{M} is a matrix given in the Appendix. The Bogoliubov modes are then given by the eigenvalue equations $\mathcal{M}\mathbf{x} = \hbar\omega\mathbf{x}$, where ω represents the excitation frequency. If all the ω 's are real, then the system is dynamically stable. Otherwise, the system is dynamically unstable with the growth rate of the instability characterized by $\text{Im}(\omega)$.

In the absence of cavity, the homogeneous ground state of a ferromagnetic ⁸⁷Rb condensate has been found to be stable against spatial modulation even in the presence of a homogeneous magnetic field [21]. This, as we shall show, will not always be the case when the cavity is introduced. To illustrate this, we numerically diagonalize \mathcal{M} to investigate the properties of Bogoliubov excitations. For the spin-1 system as

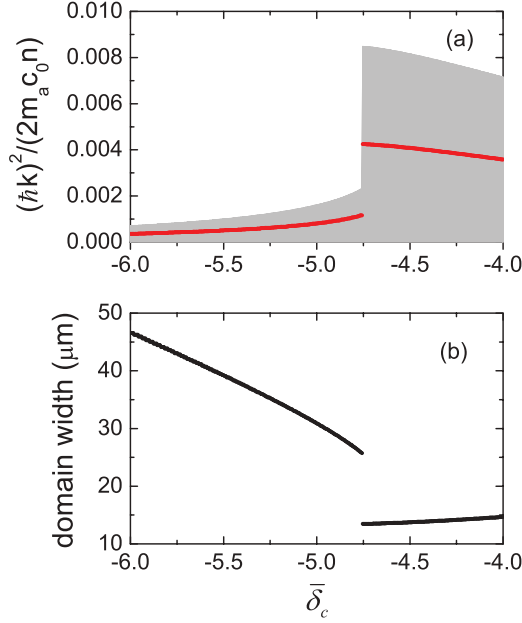


FIG. 4. (Color online) (a) The gray area shows the range of wave vector k corresponding to the unstable excitations of the self-consistent ground state of a homogeneous rubidium condensate-cavity interacting system. The red lines (top) refer to those with the maximum instability growth rate. (b) Spin-domain width versus cavity-pump detuning $\bar{\delta}_c$.

we considered here, there will be three branches of Bogoliubov excitations—two gapless branches and one gapped branch. Our numerical calculations reveal that one of the gapless branches will become unstable for certain values of the wave number k . Figure 4(a) shows the range of unstable wave numbers as the cavity-pump detuning is varied, and those with the maximum instability growth rate are represented by the red lines (top). Furthermore, the Bogoliubov eigenvectors of these most unstable modes are found to take the following form:

$$u_\alpha^T, v_\alpha^T \propto (-0.5, 0, 0.5) \text{ or } (0.5, 0, -0.5),$$

which describe the spin waves with spin angular momentum $\pm\hbar$. The exponential growth of these modes tends to induce spontaneous magnetization, and spin domain will be formed as a result of the competition between local spontaneous magnetization and the conservation of the total magnetization. The smallest size of the spin domain may be estimated by the inverse of the wave number $d_m \approx 2\pi/k_m$ where k_m is the largest unstable wave number, which is plotted in Fig. 4(b).

It is important to note that if the size of the condensate is small compared to the domain width d_m estimated above, the instability will be suppressed. Under such conditions, the SMA is expected to be valid. Conversely, when the size of the condensate becomes larger than d_m , spin-domain formation may occur.

B. Spin domain structure

Equipped with the insights gained from the study of a homogeneous condensate in the previous subsection, we are now in the position to explore the effect of cavity-induced atom-atom interaction on spin-domain formation in a trapped

condensate. For simplicity, we consider a cigar-shaped trap with a harmonic trapping potential $V_T(\mathbf{r}) = m_a[\omega_\perp^2(x^2 + y^2) + \omega_z^2 z^2]/2$ in which the transverse trap frequency ω_\perp is much higher than the longitudinal trap frequency ω_z . This allows us to introduce a longitudinal wave function $\phi_\alpha(z, t)$ via the ansatz $\psi_\alpha(\mathbf{r}, t) = \phi_\perp(x, y)\phi_\alpha(z, t)\exp(-2i\omega_\perp t)$, assuming that the transverse wave function $\phi_\perp(x, y)$ always remains in the ground state of the transverse potential. This assumption is valid when the condensate chemical potential is much less than the transverse trap frequency such that the transverse condensate wave function is frozen in the ground-state motion of the transverse trapping potential. Following the standard approach (see, e.g., Refs. [18,21]), we simplify Eqs. (1a), (1b), and (2) into a set of equations for $\phi_\alpha(z, t)$:

$$i\hbar\dot{\phi}_\pm = [\tilde{\mathcal{L}} + U_0|\alpha|^2 + \bar{c}_2(\rho_\pm + \rho_0 - \rho_\mp)]\phi_\pm + \bar{c}_2\phi_0^2\phi_\mp^*, \quad (7a)$$

$$i\hbar\dot{\phi}_0 = [\tilde{\mathcal{L}} + \bar{c}_2(\rho_+ + \rho_-)]\phi_0 + 2\bar{c}_2\phi_+\phi_-\phi_0^*, \quad (7b)$$

which describe an effective one-dimensional trapped system, where

$$\tilde{\mathcal{L}} = -\frac{\hbar^2}{2m_a}\frac{\partial^2}{\partial z^2} + \frac{m}{2}\omega_z^2 z^2 + \bar{c}_0\rho,$$

with $\rho_\alpha = |\phi_\alpha|^2$, $\rho = \rho_+ + \rho_0 + \rho_-$, and $\bar{c}_{0(2)} = c_{0(2)}m_a\omega_\perp/2\pi\hbar$.

In our calculation, we set the trap frequencies as $\omega_\perp = (2\pi)240\text{ Hz}$ and $\omega_z = (2\pi)24\text{ Hz}$ [20], and other parameters the same as before. The Thomas-Fermi radius in the z direction is then about $24\ \mu\text{m}$. In the numerical simulation, we obtain the ground state in a self-consistent manner by propagating Eq. (7) in imaginary time subject to the constraints set by the conservation of both the total particle number and the magnetization. The results are shown in Fig. 5. From the numerical simulation we find there exists a critical

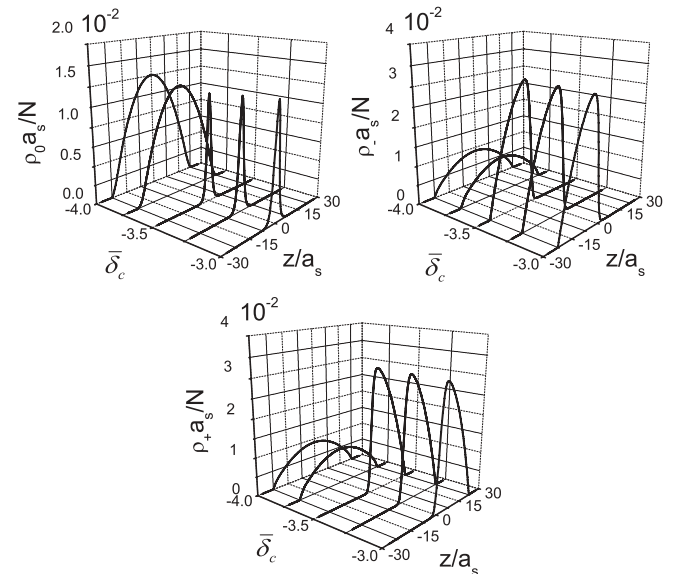


FIG. 5. The ground density profile of a ^{87}Rb condensate trapped in a unidirectional ring cavity. Here the distance z is scaled with $a_s = \sqrt{\hbar/m_a\omega_z}$ and the parameters used are specified in the main text.

value of the cavity-pump detuning $\Delta_c \approx -3.5$. The ground state exhibits a typical spin-domain structure when $\bar{\delta}_c > \Delta_c$, in which $m_g = 1$ and -1 states occupy the opposite ends of the cigar-shaped trap. While for $\bar{\delta}_c < \Delta_c$, all three spin components are completely miscible with no spin domains forming, and the ground state is well described by the SMA. This is a clear proof that the cavity light field can be used to control spin-domain formation in the condensate. The mechanism lies in the fact that the domain width can be significantly modified by tuning the cavity-pump detuning $\bar{\delta}_c$, as we have shown in Fig. 4(b). When $\bar{\delta}_c > \Delta_c$, the domain width (around $14 \mu\text{m}$) is smaller than the condensate size and spin domain can be formed. While for $\bar{\delta}_c < \Delta_c$, the domain width is larger than the size of the condensate, then the domain formation instability is suppressed.

At this point, we comment that spin domains were first observed in the ground state of a ^{23}Na antiferromagnetic condensate in the presence of the magnetic field gradient [1]. Later studies [18–20] discovered that a ferromagnetic spinor condensate initially prepared in an excited state will be subject to dynamical instability and lead to spin-domain formation, while antiferromagnetic ones are dynamically stable. The experiment of Ref. [2] displayed the spin domains formed in a quenched ^{87}Rb ferromagnetic condensate. Recent work [21] clarified that for a spin-1 condensate subject to a homogeneous magnetic field, the ground state exhibits domain formation only in antiferromagnetic condensates, but not in the ferromagnetic ones. The significance of our work here is that spin-domain structures can also be created in the ground state of a ferromagnetic condensate with the aid of a cavity. This can be traced to the effective spin-dependent atom-atom interaction induced by the cavity.

V. CONCLUSION

In conclusion, we have studied the mutual interaction of a ferromagnetic spin-1 condensate with a single-mode cavity. The intracavity light field and condensate wave functions are calculated self-consistently. The cavity-mediated effective interaction gives rise to a variety of interesting spin-dependent phenomena. Under the SMA, both the equilibrium properties and nonequilibrium dynamics are investigated in detail. We show that the system can display bistable behavior. By tuning the cavity-pump detuning, the spin-mixing dynamics can be manipulated. We also discussed the situation when the SMA becomes invalid, and found that phase transition among different spin components can occur in the ground state which leads to spin-domain structure. All these effects can be readily tested in experiments. The cavity-spinor condensate system thus provides a platform for the study of cavity nonlinear optics and the properties of spinor condensates.

VI. ACKNOWLEDGMENTS

This work is supported by the National Natural Science Foundation of China (NSFC) under Grant No. 10588402, the National Basic Research Program of China (973 Program) under Grant No. 2006CB921104, the Program of Shanghai Subject Chief Scientist under Grant No. 08XD14017, the Shanghai Leading Academic Discipline Project under Grant No. B480 (W.Z.), and by the ‘‘Chen Guang’’ project supported by Shanghai Municipal Education Commission and Shanghai Education Development Foundation (L.Z.), Fundamental Research Funds for the Central Universities (L.Z., K.Z.), and NSF (H.P., H.Y.L.), ARO (H.Y.L.), and Welch Foundation with Grant No. C-1669 (H.P.).

APPENDIX: DERIVATION OF \mathcal{M}

Inserting $\psi_\alpha = (\sqrt{n_\alpha^s} + \delta\psi_\alpha) \exp(-i\mu_\alpha^s t - i\theta_\alpha^s)$ and $\alpha = \alpha^s + \delta\alpha$ into Eqs. (1a) and (1b) where α^s is the steady-state value of Eq. (2) corresponding to the equilibrium solutions $(n_\alpha^s, \theta_\alpha^s)$, in the homogeneous case ($V_T = 0$), keeping terms up to first order in $\delta\psi_\alpha$ and $\delta\alpha$, we obtain

$$\begin{aligned} i\hbar\delta\dot{\psi}_\pm = & [-\hbar^2\nabla^2/2m_a - \mu_\pm^s + U_0|\alpha^s|^2 + 2(c_0 + c_2)n_\pm^s \\ & + (c_0 + c_2)n_0^s + (c_0 - c_2)n_\mp^s]\delta\psi_\pm \\ & + [(c_0 + c_2)n_\pm^s + c_2n_0^s \exp(-i\theta^s)]\delta\psi_\pm^* \\ & + (c_0 + c_2)\sqrt{n_0^s n_\pm^s}(\delta\psi_0 + \delta\psi_0^*) \\ & + (c_0 - c_2)\sqrt{n_-^s n_+^s}(\delta\psi_+ + \delta\psi_+^*) \\ & + 2c_2\sqrt{n_0^s n_\mp^s}\delta\psi_0 \exp(-i\theta^s) \\ & + U_0\sqrt{n_\pm^s}(\alpha^s\delta\alpha^* + \alpha^{s*}\delta\alpha), \end{aligned} \quad (\text{A1})$$

$$\begin{aligned} i\hbar\delta\dot{\psi}_0 = & [-\hbar^2\nabla^2/2m_a - \mu_0^s + (c_0 + c_2)(n_+^s + n_-^s) + 2c_0n_0^s] \\ & \times \delta\psi_0 + c_0n_0^s\delta\psi_0^* + (c_0 + c_2)[\sqrt{n_+^s n_0^s}(\delta\psi_+ + \delta\psi_+^*) \\ & + \sqrt{n_-^s n_0^s}(\delta\psi_- + \delta\psi_-^*)] + 2c_2(\sqrt{n_+^s n_-^s}\delta\psi_0^* \\ & + \sqrt{n_+^s n_0^s}\delta\psi_- + \sqrt{n_-^s n_0^s}\delta\psi_+) \exp(i\theta^s), \end{aligned} \quad (\text{A2})$$

and

$$\begin{aligned} \delta\alpha = & -\frac{iU_0V\alpha^s}{\kappa - i[\delta_c - U_0(N_+^s + N_-^s)]} [\sqrt{n_+^s}(\delta\psi_+ + \delta\psi_+^*) \\ & + \sqrt{n_-^s}(\delta\psi_- + \delta\psi_-^*)], \end{aligned} \quad (\text{A3})$$

where $V = N/n$ is the volume of the condensate and the use of Eq. (2) has been made in arriving at Eq. (A3). Finally, by combining Eqs. (A1), (A2), and (A3), we can construct matrix \mathcal{M} in a straightforward way.

- [1] J. Stenger, S. Inouye, D. M. Stamper-Kurn, H.-J. Miesner, A. P. Chikkatur, and W. Ketterle, *Nature (London)* **396**, 345 (1998).
 [2] L. E. Sadler, J. M. Higbie, S. R. Leslie, M. Vengalattore, and D. M. Stamper-Kurn, *Nature (London)* **443**, 312 (2006).

- [3] M.-S. Chang, Q. S. Qin, W. Zhang, L. You, and M. S. Chapman, *Nat. Phys.* **1**, 111 (2005).
 [4] M.-S. Chang, C. D. Hamley, M. D. Barrett, J. A. Sauer, K. M. Fortier, W. Zhang, L. You, and M. S. Chapman, *Phys. Rev. Lett.* **92**, 140403 (2004).

- [5] A. T. Black, E. Gomez, L. D. Turner, S. Jung, and P. D. Lett, *Phys. Rev. Lett.* **99**, 070403 (2007).
- [6] A. E. Leanhardt, Y. Shin, D. Kielpinski, D. E. Pritchard, and W. Ketterle, *Phys. Rev. Lett.* **90**, 140403 (2003).
- [7] H.-J. Miesner, D. M. Stamper-Kurn, J. Stenger, S. Inouye, A. P. Chikkatur, and W. Ketterle, *Phys. Rev. Lett.* **82**, 2228 (1999).
- [8] Y. Liu, S. Jung, S. E. Maxwell, L. D. Turner, E. Tiesinga, and P. D. Lett, *Phys. Rev. Lett.* **102**, 125301 (2009).
- [9] T.-L. Ho, *Phys. Rev. Lett.* **81**, 742 (1998).
- [10] T. Ohmi and K. Machida, *J. Phys. Soc. Jpn.* **67**, 1822 (1998).
- [11] B. Damski and W. H. Zurek, *Phys. Rev. Lett.* **99**, 130402 (2007); *New J. Phys.* **11**, 063014 (2009).
- [12] H. Pu, S. Raghavan, and N. P. Bigelow, *Phys. Rev. A* **61**, 023602 (2000).
- [13] W. Zhang, D. L. Zhou, M.-S. Chang, M. S. Chapman, and L. You, *Phys. Rev. A* **72**, 013602 (2005).
- [14] D. R. Romano and E. J. V. de Passos, *Phys. Rev. A* **70**, 043614 (2004).
- [15] J. Mur-Petit, *Phys. Rev. A* **79**, 063603 (2009).
- [16] C. K. Law, H. Pu, and N. P. Bigelow, *Phys. Rev. Lett.* **81**, 5257 (1998).
- [17] L. Santos, M. Fattori, J. Stuhler, and T. Pfau, *Phys. Rev. A* **75**, 053606 (2007).
- [18] N. P. Robins, W. Zhang, E. A. Ostrovskaya, and Y. S. Kivshar, *Phys. Rev. A* **64**, 021601(R) (2001).
- [19] H. Saito and M. Ueda, *Phys. Rev. A* **72**, 023610 (2005).
- [20] W. Zhang, D. L. Zhou, M.-S. Chang, M. S. Chapman, and L. You, *Phys. Rev. Lett.* **95**, 180403 (2005).
- [21] M. Matuszewski, T. J. Alexander, and Y. S. Kivshar, *Phys. Rev. A* **78**, 023632 (2008); **80**, 023602 (2009).
- [22] Q. Gu and H. Qiu, *Phys. Rev. Lett.* **98**, 200401 (2007); C. Tao and Q. Gu, *Phys. Rev. A* **79**, 023612 (2009).
- [23] F. Brennecke, T. Donner, S. Ritter, T. Bourdel, M. K. Köhl, and T. Esslinger, *Nature* **450**, 268 (2007).
- [24] Y. Colombe, T. Steinmetz, G. Dubois, F. Linke, D. Hunger, and J. Reichel, *Nature* **450**, 272 (2007).
- [25] S. Gupta, K. L. Moore, K. W. Murch, and D. M. Stamper-Kurn, *Phys. Rev. Lett.* **99**, 213601 (2007).
- [26] K. W. Murch, K. L. Moore, S. Gupta, and D. M. Stamper-Kurn, *Nature Phys.* **4**, 561 (2008).
- [27] F. Brennecke, S. Ritter, T. Donner, and T. Esslinger, *Science* **322**, 235 (2008); S. Ritter, F. Brennecke, K. Baumann, T. Donner, C. Guerlin, and T. Esslinger, *Appl. Phys. B* **95**, 213 (2009).
- [28] P. Horak, S. M. Barnett, and H. Ritsch, *Phys. Rev. A* **61**, 033609 (2000); P. Horak and H. Ritsch, *ibid.* **63**, 023603 (2001).
- [29] P. Domokos and H. Ritsch, *Phys. Rev. Lett.* **89**, 253003 (2002); G. Szirmai and P. Domokos, *Eur. Phys. J. D* **48**, 127 (2008).
- [30] J. M. Zhang, W. M. Liu, and D. L. Zhou, *Phys. Rev. A* **77**, 033620 (2008); **78**, 043618 (2008).
- [31] M. G. Moore and P. Meystre, *Phys. Rev. A* **59**, R1754 (1999); M. G. Moore, O. Zobay, and P. Meystre, *ibid.* **60**, 1491 (1999).
- [32] J. Larson, B. Damski, G. Morigi, and M. Lewenstein, *Phys. Rev. Lett.* **100**, 050401 (2008); J. Larson, S. Fernández-Vidal, G. Morigi, and M. Lewenstein, *New J. Phys.* **10**, 045002 (2008).
- [33] R. Kanamoto and P. Meystre, *Phys. Rev. Lett.* **104**, 063601 (2010); K. Zhang, W. Chen, M. Bhattacharya, and P. Meystre, *Phys. Rev. A* **81**, 013802 (2010); W. Chen, K. Zhang, D. S. Goldbaum, M. Bhattacharya, and P. Meystre, *ibid.* **80**, 011801(R) (2009).
- [34] I. B. Mekhov, C. Maschler, and H. Ritsch, *Nat. Phys.* **3**, 319 (2007); *Phys. Rev. Lett.* **98**, 100402 (2007); I. B. Mekhov and H. Ritsch, *ibid.* **102**, 020403 (2009).
- [35] L. Zhou, H. Pu, H. Y. Ling, and W. Zhang, *Phys. Rev. Lett.* **103**, 160403 (2009).
- [36] L. Zhou, W. Zhang, H. Y. Ling, L. Jiang, and H. Pu, *Phys. Rev. A* **75**, 043603 (2007).
- [37] R. W. Boyd, *Nonlinear Optics*, 2nd ed. (Academic Press, Boston, 2003).
- [38] λ_a is estimated with $a_0 = 101.8a_B$, $a_2 = 100.4a_B$ for ^{87}Rb atoms, the cavity decay rate $\kappa = (2\pi)100$ KHz, and a typical atomic density $n = 1.9 \times 10^{14} \text{ cm}^{-3}$.
- [39] R. Bonifacio and P. Meystre, *Opt. Commun.* **29**, 131 (1979); K. Zhang, W. Chen, and P. Meystre, *ibid.* **283**, 665 (2010).